JOURNAL OF GEOPHYSICAL RESEARCH: SOLID EARTH, VOL. 118, 3848–3859, doi:10.1002/jgrb.50283, 2013

Time-variable gravity signal in Greenland revealed by high-low satellite-to-satellite tracking

M. Weigelt,[1] T. van Dam,[1] A. Jäggi,[2] L. Prange,[2] M. J. Tourian,[3] W. Keller,[3] and N. Sneeuw[3]

Received 19 February 2013; revised 1 July 2013; accepted 4 July 2013; published 30 July 2013.

[1] In the event of a termination of the Gravity Recovery and Climate Experiment (GRACE) mission before the launch of GRACE Follow-On (due for launch in 2017), high-low satellite-to-satellite tracking (hl-SST) will be the only dedicated observing system with global coverage available to measure the time-variable gravity field (TVG) on a monthly or even shorter time scale. Until recently, hl-SST TVG observations were of poor quality and hardly improved the performance of Satellite Laser Ranging observations. To date, they have been of only very limited usefulness to geophysical or environmental investigations. In this paper, we apply a thorough reprocessing strategy and a dedicated Kalman filter to Challenging Minisatellite Payload (CHAMP) data to demonstrate that it is possible to derive the very long-wavelength TVG features down to spatial scales of approximately 2000 km at the annual frequency and for multi-year trends. The results are validated against GRACE data and surface height changes from long-term GPS ground stations in Greenland. We find that the quality of the CHAMP solutions is sufficient to derive long-term trends and annual amplitudes of mass change over Greenland. We conclude that hl-SST is a viable source of information for TVG and can serve to some extent to bridge a possible gap between the end-of-life of GRACE and the availability of GRACE Follow-On.

Citation: Weigelt, M., T. van Dam, A. Jäggi, L. Prange, M. J. Tourian, W. Keller, N. Sneeuw (2013), Time-variable gravity signal in Greenland revealed by high-low satellite-to-satellite tracking, *J. Geophys. Res. Solid Earth*, *118*, 3848–3859, doi:10.1002/jgrb.50283.

1. Introduction

[2] In the last decade, temporal variations of the gravity field (TVG) have become one of the most ubiquitous and valuable sources of global information for geophysical and environmental studies. Since 2002, the Gravity Recovery and Climate Experiment (GRACE) mission [*Tapley et al.*, 2004] has delivered monthly snapshots of the gravity field that are used to map the redistribution of mass within the Earth's fluid layers (atmosphere, continental water, oceans, ice, and solid Earth). As the value of any geophysical or environmental record is proportional to the length of the time series, it is imperative that the TVG time series is not interrupted (or even worse stopped) as some geophysical phenomena, e.g., postglacial rebound (PGR), are only just beginning to be observable. However, GRACE has already outlived its predicted lifetime by more than 5 years. Engineers at the Center for Space Research (CSR) at the University of Texas at Austin, at the German Research Centre for Geosciences (GFZ) and NASA's Jet Propulsion Laboratory are taking every measure necessary to keep GRACE alive until the GRACE Follow-On mission (GRACE-FO) [*Flechtner et al.*, 2013] is operational. But, the reality is that GRACE can fail at any time due to the meanwhile more than double lifetime of the mission.

[3] In the worst case of an immediate failure of GRACE, a data gap of 4 years (provided that GRACE-FO will be launched in 2017) will arise in our observations of the global TVG. The question is then: What is the backup plan? Do we have any possibility to measure the global TVG field in the gap between a loss of GRACE and the time GRACE-FO becomes operational? The only other dedicated gravity field missions currently in space is the Gravity field and steady state Ocean Circulation Explorer (GOCE) [*European Space Agency*, 1999]. Beyond, the upcoming Swarm mission [*European Space Agency*, 2004] is a possible candidate since the three satellites have a close resemblance to the satellite of the former CHallenging Minisatellite Payload (CHAMP) mission. Unfortunately, neither carries the low-low satellite-to-satellite tracking (ll-SST) ultra-precise K-band observation system of GRACE. However, as we demonstrate here, it is possible to derive the time-variable gravity from GPS-derived low Earth orbiter (LEO) orbits, a concept known as high-low satellite-to-satellite tracking (hl-SST).

[1]Faculty of Science, Technology, and Communication, Research Unit of Engineering Science, University of Luxembourg, Luxembourg.
[2]Astronomical Institute, University of Bern, Bern, Switzerland.
[3]Institute of Geodesy, University of Stuttgart, Stuttgart, Germany.

Corresponding author: M. Weigelt, Faculty of Science, Technology, and Communication, Research Unit of Engineering Science, University of Luxembourg, 6 rue Richard Coudenhove-Kalergi, 1359 Luxembourg, Luxembourg. (matthias.weigelt@uni.lu)

2169-9313/13/10.1002/jgrb.50283

Table 1. Summary of Dynamical and Measurement Models Employed for the GNSS Orbit Determination[a]

Model Type	Applied Model or Convention
Reference frame[b]	ITRF2005/IGS05; *Altamimi et al.* [2007]
Subdaily pole	IERS2003; *McCarthy* [2004]
Solid Earth tides	IERS2003; *McCarthy* [2004]
Meanpole convention	IERS2003; *McCarthy* [2004]
Ocean tides	CSR3.0
Gravity field model[c]	JGM3, $L^{max} = 12$; *Tapley et al.* [1996]
Antenna phase center	Absolute model; *Schmid et al.* [2007]
Tropospheric mapping	Global mapping function (GMF)
Radiation pressure[d]	Improved CODE RPR model
Phase-windup	Applied
Ocean tidal loading[e]	FES2004; *Lyard et al.* [2006]

[a]IERS, International Earth Rotation and Reference Systems Service.
[b]ITRF, International Terrestrial Reference Frame.
[c]JGM, Joint Gravity Model.
[d]RPR, Radiation PRessure.
[e]FES, Finite Element Solution.

[4] CHAMP was based on the hl-SST concept and was supposed to contribute to the efforts of Satellite Laser Ranging (SLR) in determining the gravity field by delivering observations of the time variability of the long-wavelength features of the gravity field [*Reigber et al.*, 2001]. Several attempts have been made but success has been very limited [e.g., *Sneeuw et al.*, 2002; *Qiang and Moore*, 2005]. Those authors concluded that the poorer accuracy of the GPS-observations in hl-SST missions (approximately a factor of 1000) is the primary limiting factor. Often, temporal variations have only been identified in combination with Satellite Laser Ranging (SLR) observations [e.g., *Cheng et al.*, 2002]. The first realistic solutions based solely on CHAMP data have been achieved by *Prange* [2010] using the so-called stacking solutions. Monthly estimates have been derived by analyzing residuals to the mean solution Astronomical Institute of the University of Bern (AIUB)-CHAMP03s [*Prange*, 2010]. Then, results of one particular month are collected over several years (i.e., all Januaries, Februaries, etc.) and combined yielding a mean annual solution which already showed typical patterns of geophysical phenomena. Also the coestimation of trends, annual, and semiannual variations of the spherical harmonic coefficients enabled the derivation of a realistic mean annual solution. Recently, *Lin et al.* [2012] estimated time variability from hl-SST observations of the COSMIC satellite formation.

[5] In this paper, we demonstrate that it is possible to derive the long-wavelength time-variable gravity field from hl-SST observations. This is achieved by (1) a thorough reprocessing of the GPS-observations, and (2) the application of a dedicated Kalman filter after the spherical harmonic analysis which is able to recover interannual variabilities. We show that we are able to resolve the time-variable gravity field up to approximately degree and order 10. This resolution allows us to derive the prominent features of the mass change trends over Greenland.

[6] The paper outlines the GPS processing and the Kalman filter design in section 2. It focuses then on the time-variable signal in Greenland (section 3.1). Results are externally validated with the GRACE CSR release 5 monthly solutions and loading time series of four GPS stations (section 3.3).

2. Methodology

[7] A combination of three important procedures enables the recovery of the time-variable gravity field from high-low satellite-to-satellite missions. These procedures include (1) GPS processing, (2) gravity field recovery, and (3) Kalman filtering. Each of these processing steps will be discussed in the following subsections.

2.1. GPS Reprocessing

[8] Modern gravity missions make all use of GPS-based hl-SST for precise orbit determination (POD), observation time-tagging, and the extraction of the long-wavelength part of the Earth's gravity field. GPS orbits and high-rate GPS clock corrections are thus a prerequisite to process data from any of the modern gravity missions. Orbit and clock products provided by the International GNSS Service (IGS) [*Dow et al.*, 2005], e.g., the final product line, are promising the highest possible accuracy and reliability. The global analysis centers of the IGS, however, frequently adopt background model and processing changes to steadily improve the quality of the operational solutions. As a consequence, reprocessing efforts are unavoidable to obtain homogeneous long-time product series as otherwise long-time series of the IGS products are becoming inevitably inconsistent [*Steigenberger et al.*, 2006].

2.1.1. Reprocessed GPS Orbit Solutions

[9] A reprocessing tailored to the needs of global gravity field determination was performed at the Astronomical Institute of the University of Bern (AIUB) by *Prange* [2010]. Data of the global IGS network covering the years 2003 to 2009 were processed according to a scheme similar to that used for the operational solution computed at the Center for Orbit Determination in Europe (CODE) [*Dach et al.*, 2009]. The adopted background models are conforming to the models adopted by the IGS on 5 November 2006 (GPS week 1400) when switching from the relative to the absolute antenna phase center model [*Schmid et al.*, 2007] and are summarized in Table 1. The generated products are GPS satellite orbits, station coordinates, troposphere parameters, and Earth rotation parameters.

2.1.2. Reprocessed Clock Solutions

[10] The CHAMP (and GRACE) Level-1b GPS hl-SST data are both available with a sampling rate of 10 s. In order to exploit the full amount of hl-SST data for gravity field recovery, GPS satellite clock corrections need to be available with the sampling rate of at least that of the CHAMP data to avoid clock interpolation. CODE has started to deliver 30 s GPS clock corrections already since GPS week 1265 (4 April 2004) as part of the CODE final clock product [*Hugentobler*, 2004] according to a procedure described by *Bock et al.* [2009], but 5 s GPS clock corrections have been delivered since GPS week 1478 (3 May 2008) only [*Schaer and Dach*, 2008]. Data from the IGS high-rate network have thus been used to generate a homogeneous series of high-rate GPS clock corrections covering the years 2003 till 2009. In the year 2003, the number of IGS high-rate stations was still limited. The number of station increases from about 30 in 2003 to approximately 80 by the end of 2006. Therefore, non-IGS stations were included in the processing as well. More details can be found in *Prange* [2010, chapter 5].

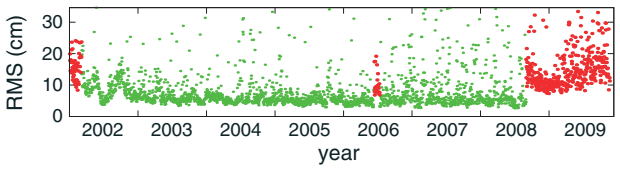

Figure 1. Daily 3-D RMS of the difference between the kinematic and reduced-dynamic CHAMP orbits. Green: up to 10 GPS satellites tracked. Red: up to eight (early 2002) or seven (mid 2006, since late 2008) GPS satellites tracked.

2.1.3. CHAMP Kinematic Orbit Determination

[11] Kinematic LEO orbits are determined at the observation epochs of the GPS hl-SST data by a precise point positioning approach [*Zumberge et al.*, 1997] with GPS orbits and clock corrections introduced as known. The kinematic LEO orbits are represented by three coordinates per measurement epoch and are determined in a standard least squares adjustment process of GPS observations together with other relevant parameters [*Švehla and Rothacher*, 2005]. In order to fully exploit kinematic LEO POD and the subsequent gravity field recovery, a precise modeling of the antenna phase center location is mandatory [*Jäggi et al.*, 2009]. Elevation-dependent weighting was used to process the full amount of 10 s GPS data for CHAMP, because hl-SST data are the primary observable for gravity field recovery. Reduced-dynamic orbit solutions were computed as well, but are only used for the identification and removal of outlying kinematic positions.

[12] Figure 1 shows the daily root-mean-square (RMS) of the differences between the kinematic and reduced-dynamic CHAMP orbits. As kinematic orbits are more affected by data gaps and outliers due to a much smaller number of observations per estimated parameter, the RMS values shown in Figure 1 primarily indicate the quality of the kinematic orbits. Compared with the reduced-dynamic orbits, the RMS of the difference varies mostly between 4 and 6 cm.

[13] A clear degradation of the kinematic positions is recognized at the beginning and toward the end of the analyzed time period, which may be attributed to receiver firmware changes. The maximum number of tracked GPS satellites was set to 10 for most of the time between mid 2002 and late 2008. In summer 2006, however, the receiver was temporarily switched to its redundant board for the first time. From mid 2006 onward, the receiver was switched back to its main board, but was affected by clock steering problems related to the extended mission duration (G. Michalak, German Research Centre for Geoscience, private communication, 2008). This is not critical for orbit determination as large receiver clock corrections are correctly handled within the Bernese Software as required, e.g., for the processing of GOCE GPS data [*Bock et al.*, 2011]. On 5 October 2008, the receiver was eventually switched back again to its redundant board and tracked only up to seven GPS satellites simultaneously. As only kinematic positions based on at least five GPS observations are accepted, data screening started to become a challenge. The problem was additionally aggravated by data gaps in the high-rate GPS clock corrections, e.g., due to incomplete 1 Hz receiver-independent exchange observation files. Since 5 October 2008, GPS satellite clock corrections were thus allowed to be interpolated in order not to loose large amounts of GPS observations. Despite all these measures, the series of kinematic CHAMP positions is governed by a significantly larger number of data gaps and a higher RMS value [*Prange*, 2010].

2.2. Gravity Field Recovery

[14] Depending on the gravity field recovery approach, kinematic positions need to be differentiated or variational equations have to be integrated. Here, the so-called acceleration approach [*Reubelt*, 2008] is employed but other methods like the short-arc approach [*Mayer-Gürr et al.*, 2005] or the Celestial Mechanics approach [*Beutler et al.*, 2010] will give a very similar performance. The acceleration approach is based on Newton's equation of motion in the inertial frame

$$\nabla V = \ddot{\vec{x}} - \vec{f}_{\text{3rdbody}} - \vec{f}_{\text{tides}} - \vec{f}_{\text{rel}} - \vec{f}_{\text{grav}} - \vec{f}_{\text{ng}} \qquad (1)$$

where ∇V is the gradient of the Earth gravitational potential V, and $\ddot{\vec{x}}$ are the accelerations of the satellite which are derived by numerical differentiation from the aforementioned kinematic positions. Third-body related forces $\vec{f}_{\text{3rdbody}}$, tidal forces $\vec{f}_{\text{tides}}$, relativistic corrections $\vec{f}_{\text{rel}}$, and all (time-variable) gravitational changes $\vec{f}_{\text{grav}}$, which cannot

Table 2. Data and Models Used for the Generation of the Solutions CHAMP v1 and v2: The Reference for IERS2003 Is *McCarthy* [2004] and for IERS2010 Is *Petit and Luzum* [2010]

	CHAMP v1	CHAMP v2
Position data	*Švehla and Rothacher* [2005]	*Prange* [2010]
Antenna phase center model	no	yes
Approach	energy balance	acceleration
Third-body forces	point masses for Sun and Moon coordinates from DE405	
Solid Earth tide	IERS2003	IERS2010
Pole tide	IERS2003	IERS2010
Ocean tide	FES2004; *Lyard et al.* [2006]	
Ocean pole tide	IERS2003	IERS2010
Atmospheric tide	no	N1-model; *Biancale and Bode* [2006]
Dealiasing product	no	AOD1B Release 04; *Flechtner* [2007]
Relativistic corr.	IERS2003	IERS2010
Accelerometer data	yes	no
→ Calibration param.	bias: daily	-
	scale: 1 per month	-

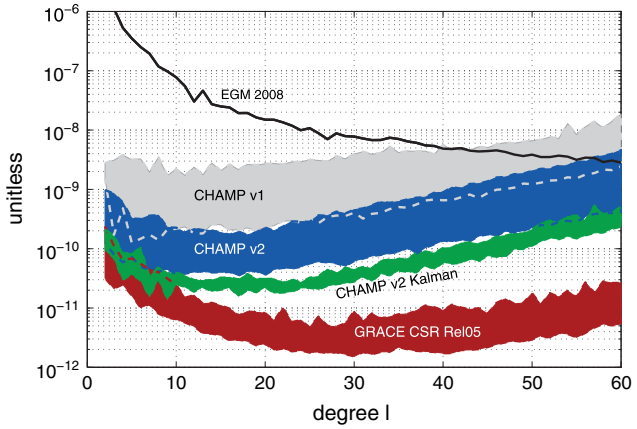

Figure 2. Spread of the monthly gravity field solutions: CHAMP before the reprocessing (v1, gray), after the reprocessing (v2, blue), and after the Kalman filtering (green) in comparison to GRACE CSR release 05 (red).

be estimated but need to be reduced (e.g., dealiasing products for correction of nontidal effects), are subtracted. The third column (CHAMP v2) in Table 2 gives an overview of the applied correction models. All calculations are performed per unit mass, and the 6-hourly spherical harmonic coefficients of the atmospheric and ocean dealiasing (AOD) product [*Flechtner*, 2007] are linearly interpolated to the epoch of calculation. Although some of the effects might arguably be insignificant, they have been included in order to be consistent with a standard GRACE data processing. Nongravitational forces $\vec{f}_{\mathrm{ng}}$ caused by, e.g., atmospheric drag or solar radiation pressure are measured by the accelerometer onboard CHAMP. However, we did not make use of this data as it turned out to not improve the solutions at the current stage. This property is specific to the acceleration approach and is discussed in more detail in *Reubelt* [2008]. Other solutions, e.g., from CSR or GFZ are based on different approaches and often require the usage of the accelerometer information.

[15] The gravitational potential V is developed into a spherical harmonic (SH) expansion [*Heiskanen and Moritz*, 1967]. The unknowns are the SH-coefficients $\bar{C}_{lm}$ and $\bar{S}_{lm}$ to degree and order 120 which are estimated monthly in a least squares adjustment. It is important to note that the solutions have been derived without the need for any a priori model and/or regularization. The monthly solutions are also used to derive the static field ULux-CHAMP2013s comprising the full period of available data from January 2003 till December 2009.

[16] Figure 2 shows the spread of the difference between the computed (monthly) gravity field with respect to the static mean field EGM2008 [*Pavlis et al.*, 2012] in terms of dimensionless degree RMS of SH-coefficient differences. The visualization is limited here to degree 60 in order to focus on the long-wavelength content. The spread is defined by the minimum and maximum difference to EGM2008. Note that this difference contains both errors and time-variable gravity field. As a guidance, the GRACE CSR Release 05 solution is given which we call for simplicity GRACE solution in the following. Since time-variable gravity signals typically exhibit an inverse power law behavior, the decay of the spread till degree $l \approx 30$–40 can—roughly speaking—be seen as the observable time-variable gravity field, whereas the increasing spread beyond this point can be considered errors.

[17] The benefit of the reprocessing is demonstrated by comparing the CHAMP v2 solution in blue to a previous solution called CHAMP v1 in gray. The solution CHAMP v1 has been derived based on 2 years of CHAMP data for the period of April 2002 to February 2004, which have been provided by the Institute for Astronomical and Physical Geodesy, Technical University Munich [*Švehla and Rothacher*, 2005]. More details about this data set can be found in Table 2 and in *Weigelt* [2007]. The gain is approximately 1 order of magnitude over the whole range of the spectrum. The comparison to the GRACE solution reveals that before the reprocessing, the CHAMP solutions were simply not accurate enough to reveal time variability of the gravity field. However, with the reprocessing, the spread of CHAMP v2 starts to intersect with the low degree components of the GRACE solutions, i.e., now time variability comes into CHAMP's sensitivity range.

[18] Time variability is reflected by sinusoidal signals in the time series of a single SH-coefficient. In Figure 3, time series of spherical harmonic coefficients from degree two to six are shown; sine coefficients with a negative order and cosine coefficients with a positive order. Comparing the "raw" time series of the CHAMP v2 solution (light blue) to the GRACE solution time series (red) shows that despite the improvements, the CHAMP time series is still dominated by noise.

[19] *Prange* [2010] made use of the redundancy given by the 7 years of data and was able to estimate mean annual models, but these are not able to take interannual variability into account. The problem is illustrated in Figure 4. The red curve is the time series for coefficient $\bar{S}_{44}$ taken from the GRACE solution. The black curve is the least squares fit to the model comprising a bias, trend, and the annual frequency given as

$$\bar{x}(t) = \bar{a}_0 + \bar{a}_1(t - t_0) + \bar{a}_2 \cos(2\pi\,(t - t_0)) + \bar{a}_3 \sin(2\pi\,(t - t_0)) \quad (2)$$

where t is given in years, t_0 is the first epoch of the time series, and $a_0 \ldots a_3$ are the unknown coefficients. It is apparent that the model is not able to represent variations in the amplitude and phase of the GRACE time series properly. The amplitude and phase of the GRACE time series are varying with time, and a fixed frequency model as the one given in equation (2) is not able to take these variations into account. Unfortunately, the limited length of the time series and the sampling frequency of 1 month prevents the expansion of equation (2) to account for additional near-annual frequencies.

2.3. Kalman Filtering

[20] One approach to mitigate the problem is to apply a Kalman filter [e.g., *Gelb*, 1974]. The mean model could serve as the prediction, which is updated with the observed value of the SH-coefficient. Here, the procedure is slightly different and we follow closely the concept outlined in *Davis et al.* [2012]. First, the time series is considered time

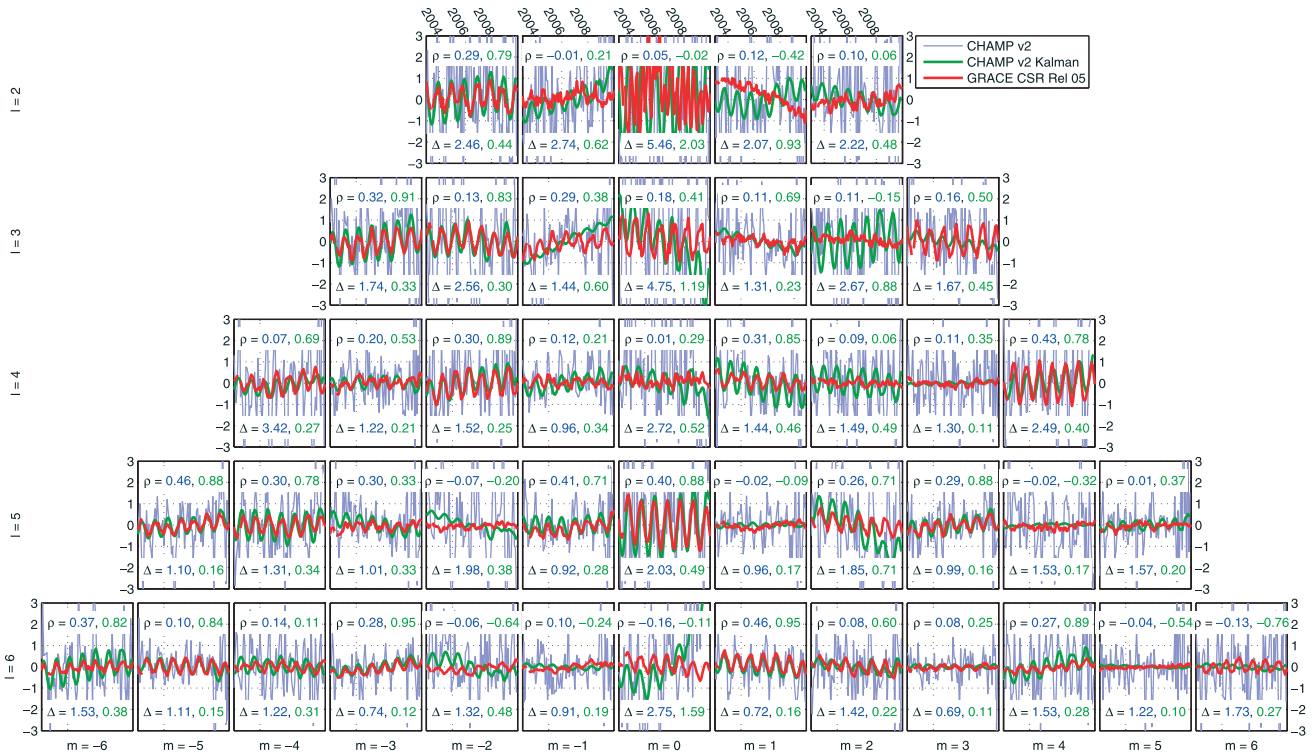

Figure 3. Time series of the spherical harmonic coefficients before (light blue) and after Kalman filtering (green); CSR GRACE release 05 for comparison in red. Cosine coefficients are shown with a positive order m and sine coefficients with a negative order. The coefficient ρ describes the correlation of the two CHAMP time series with the GRACE time series given in their respective color. Δ denotes the RMS of the difference between each CHAMP solution and GRACE.

variant and consisting of a deterministic part $\bar{x}(t)$ described by equation (2) and a zero-mean stochastic component $\delta x(t)$.

$$x(t) = \bar{x}(t) + \delta x(t) \tag{3}$$

$$\delta x(t) = \delta a_1 (t - t_0) + \delta a_2 \cos(2\pi\,(t - t_0)) + \delta a_3 \sin(2\pi\,(t - t_0)) \tag{4}$$

The deterministic part is described by the mean model in equation (2). The unknown parameters $\bar{a}_0 \ldots \bar{a}_3$ are estimated separately for each time series of SH-coefficients in a least squares adjustment. Using the CHAMP time series avoids on the one hand the contamination with any *a priori* information, e.g., from GRACE or models, and on the other hand makes the aforementioned optimal use of the redundancy as the complete time series of 7 years contributes to the determination of the parameter. Essentially, the prediction model correlates closely with the mean models of *Prange* [2010] though it is derived in a different way. The observations (the original time series of a single SH-coefficient) are reduced by the mean model, and the residuum is seen as the observations of a stochastic zero-mean process which is described by the parameters $\delta a_1 \ldots \delta a_3$. They are estimated by the Kalman filter whereas their initial values are set to zero.

[21] The process noise in the concept of the Kalman filter describes the amount of error in the prediction model which is here implicitly the deviation of the mean model from the true time-variable signal. However, the time-variable gravity signal is subject to the investigation and thus unknown. One possibility would be to use the differences between the mean model and GRACE or between the mean model and geophysical models of time-variable gravity field. But this introduces *a priori* information and biases the solution toward GRACE and the models, respectively. It can be circumvented by stochastically describing the process noise as a random walk process with zero mean. *Davis et al.* [2012] discuss the suitability of this type of model for geodetic time series and refer to as stochastic seasonal process. Practically, this is achieved by integrating a random sequence

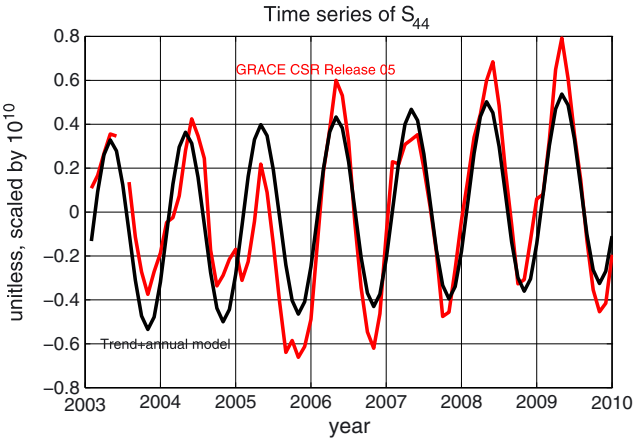

Figure 4. Time series of $\bar{S}_{44}$: GRACE CSR Release 05 in red; trend+annual fit in black; bias/mean subtracted.

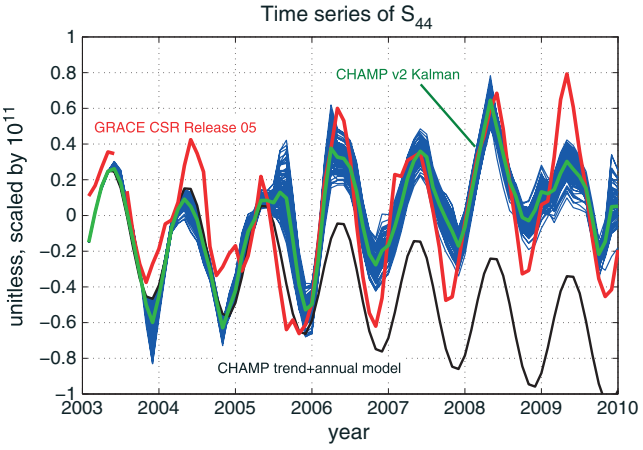

Figure 5. Example of the Kalman filtering for $\bar{S}_{44}$: mean model in black, ensemble of 100 solutions in blue, average of the ensemble in green, and GRACE CSR release 05 for comparison in red.

drawn from a Gaussian distribution. The first predicted value in the first time step of the Kalman filter is then achieved by adding the process noise to the initial value. The prediction is then updated by the first (residual) observation using the Kalman gain factor. The procedure is continued and the estimated values $\delta a_1 \ldots \delta a_3$ for each epoch are used to calculate the estimated residual time series which is added to the mean model. Additionally and in order to minimize a possible dependency on the used sequence of random numbers, we employ an ensemble approach, i.e., the estimation is repeated for different random sequences of the process noise. It results in an ensemble of solutions, which are averaged.

[22] As an example, the time series for $\bar{S}_{44}$ is shown in Figure 5. The blue curves comprise the ensemble of 100 separate solutions of the Kalman filtering, which are averaged (green curve) and used as the filtered time series. The spread of the blue curve indicates the dependency on the choice of the process noise instances. Nevertheless, the general behavior follows the signal curve designated here by GRACE in red. The mean model derived from the CHAMP v2 time series in black is shown for comparison. The filtered time series is able to follow the GRACE solution much closer than the mean model. The best performance is achieved in the years 2005 till 2008. Before, CHAMP has a lower sensitivity due to its higher orbit and from October 2008 the decreased performance due to the aforementioned switch to the redundant board of the GPS receiver is visible.

[23] The degree RMS of the difference between the Kalman-filtered monthly solutions and the static mean field EGM2008 is added to Figure 2 in green. The filtering reduces the spread considerably and gives an additional gain of half an order of magnitude. Till approximately degree 10, the CHAMP v2 Kalman solution is located within the margins of the GRACE monthly solutions. Beyond, the CHAMP v2 Kalman solutions follow the general behavior of the CHAMP v2 solution but at a reduced error level. This is an indication of the robustness of the Kalman filter procedure, i.e., its primary impact is the reduction of noise.

[24] Figure 3 shows the improved time series of CHAMP due to the filtering process in green. The correlation between the two CHAMP solutions and the GRACE solution is given at the top of each panel and is denoted by ρ in their respective colors. Generally and with only few exceptions, the correlation coefficients with respect to the GRACE solution increase. The maximum increase is achieved for $\bar{S}_{33}$ where ρ improves from 0.32 to 0.91. For $\bar{C}_{21}$, the correlation decreases as the algorithm is not able to identify the long-term trend.

[25] The RMS of the difference of CHAMP v2 Kalman solution to the GRACE solution, shown at the bottom of each panel and denoted by Δ, is reduced drastically for all coefficients compared with the unfiltered solutions. The reduced sensitivity from October 2008 is again visible, e.g., in coefficient $\bar{S}_{21}$ or $\bar{C}_{40}$. The coefficients $\bar{S}_{21}$, $\bar{C}_{22}$, $\bar{C}_{30}$, and $\bar{S}_{31}$ show unrealistic trends, which are caused by strong trends in the "raw" time series or by outliers. One of the causes of these outliers is sparse ground track coverage while the satellite passed through several repeat orbits, see *Weigelt et al.* [2013] for details. Other causes are, e.g., a poor(er) data availability or the aforementioned switch to the redundant board. Also the amplitude of $\bar{C}_{21}$ and $\bar{C}_{32}$ are of poor quality due to oscillations in the observed time series. Similar to early results from GRACE, $\bar{C}_{20}$ shows unrealistic high oscillations which is why we replace this value by SLR estimates in the following section. Yet, strong improvements are visible and high frequency noise is vastly reduced. Also the ability of the procedure to detect interannual variability can be seen, e.g., at the coefficients $\bar{S}_{32}$ or $\bar{S}_{44}$.

[26] The Kalman-filtered solutions are provided to degree and order 60. Due to the reduced sensitivity of the hl-SST observations, it is not necessary to provide the full solution till degree and order 120 but the choice is also sufficiently high in order to avoid truncation errors. The data are available at the International Centre for Global Earth Models (ICGEM) hosted at the German Research Centre for Geosciences and at the Global Geophysical Fluid Center (http://icgem.gfz-potsdam.de/ICGEM/ICGEM.html).

3. Mass Variations in Greenland

[27] An interruption of the time series provided by GRACE would be a major setback in quantifying mass variations. We investigate the ability of hl-SST to recover the trend and annual signal globally and focus especially on Greenland. Similar to the data processing in case of GRACE, we use Gaussian filters with different radii in order to suppress short-wavelength noise in the spatial domain [*Wahr et al.*, 1998]. In the comparison within this section, filtering is always applied equally to the CHAMP and the GRACE CSR release 05 solutions. Generally, solutions are restricted to a lower degree than in case of GRACE due to the lower sensitivity of hl-SST to time-variable gravity signals and the elevated noise level, cf. Figure 2.

3.1. Global Time-Variable Gravity

[28] Before focusing on Greenland, we briefly analyze the global performance of the CHAMP solution. All solutions in this section have been filtered using a Gaussian filter of 1000 km half-wavelength. Figure 6 shows the trend, the amplitude, and phase of the annual signal of the Kalman-filtered CHAMP solution and for comparison, the GRACE solution. The parameters are determined by fitting the model

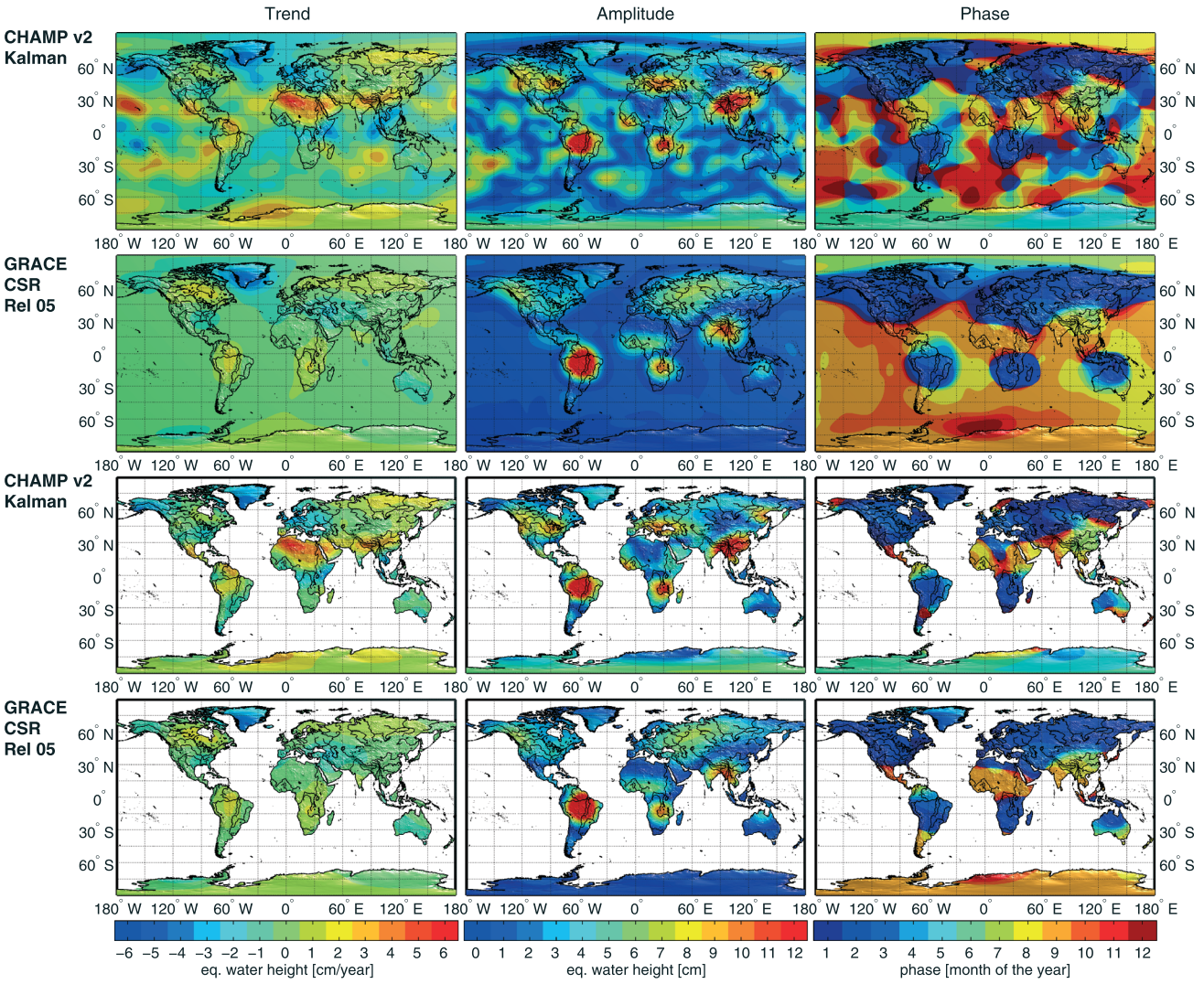

Figure 6. Trend, amplitude, and phase for (first row) CHAMP v2 with Kalman filtering and (second row) GRACE (CSR and Rel05) in terms of equivalent water height; (third and fourth rows) the same pictures are shown with a land-ocean mask.

described by equation (2) into each pixel ($\approx 0.5° \times 0.5°$). Note that at this point, no dealiasing products have been added back to the gravity fields. This omission represents a source of (small) deviations as the CHAMP solutions are based on release 4, whereas the GRACE solutions are based on release 5 of the AOD product. Due to the aforementioned problems with the sensitivity of CHAMP and the switch to the redundant board, our comparison is limited to the period January 2004–October 2008.

[29] The results in Figure 6 show that CHAMP has a higher noise level than the GRACE solution. This is especially evident over the oceans where the signal is relatively small compared to the strong hydrological induced signals on land, e.g., in the Amazon basin. The trends in the figures in the left column show good agreement for Greenland, but artificial trends in northern Africa and over some spots in the ocean can be observed. The spurious trends can be traced back to erroneous drifts in the SH-coefficients, particularly in $\bar{C}_{60}$, which exhibits a strong quadratic drift (see also Figure 3). The same drifts are visible in the unfiltered time series, i.e., the Kalman filter is not able to extract the signal content from the unfiltered time series. The results indicate that the standard deviation of the estimated SH-coefficients is an imperfect description of its error and too optimistic. This is not surprising as the true error information of the instruments is not available and thus a full error propagation is not possible. In addition, estimates of the errors induced by imperfect background models are not available and thus cannot be considered.

[30] The amplitude of the annual signal in the middle column of Figure 6 shows the strongest of the well-known continental water storage patterns, e.g., in the Amazon basin, in the Zambesi area or East of India. At the same time, we observe a higher noise level that explains the erroneous patterns in North-America, Europe, and North-East Asia. The corresponding CHAMP and GRACE phase patterns in the right column agree particularly well in the Northern Hemisphere.

[31] As the noise level appears dominant on the oceans, we added the same two figures masking out the oceans in the

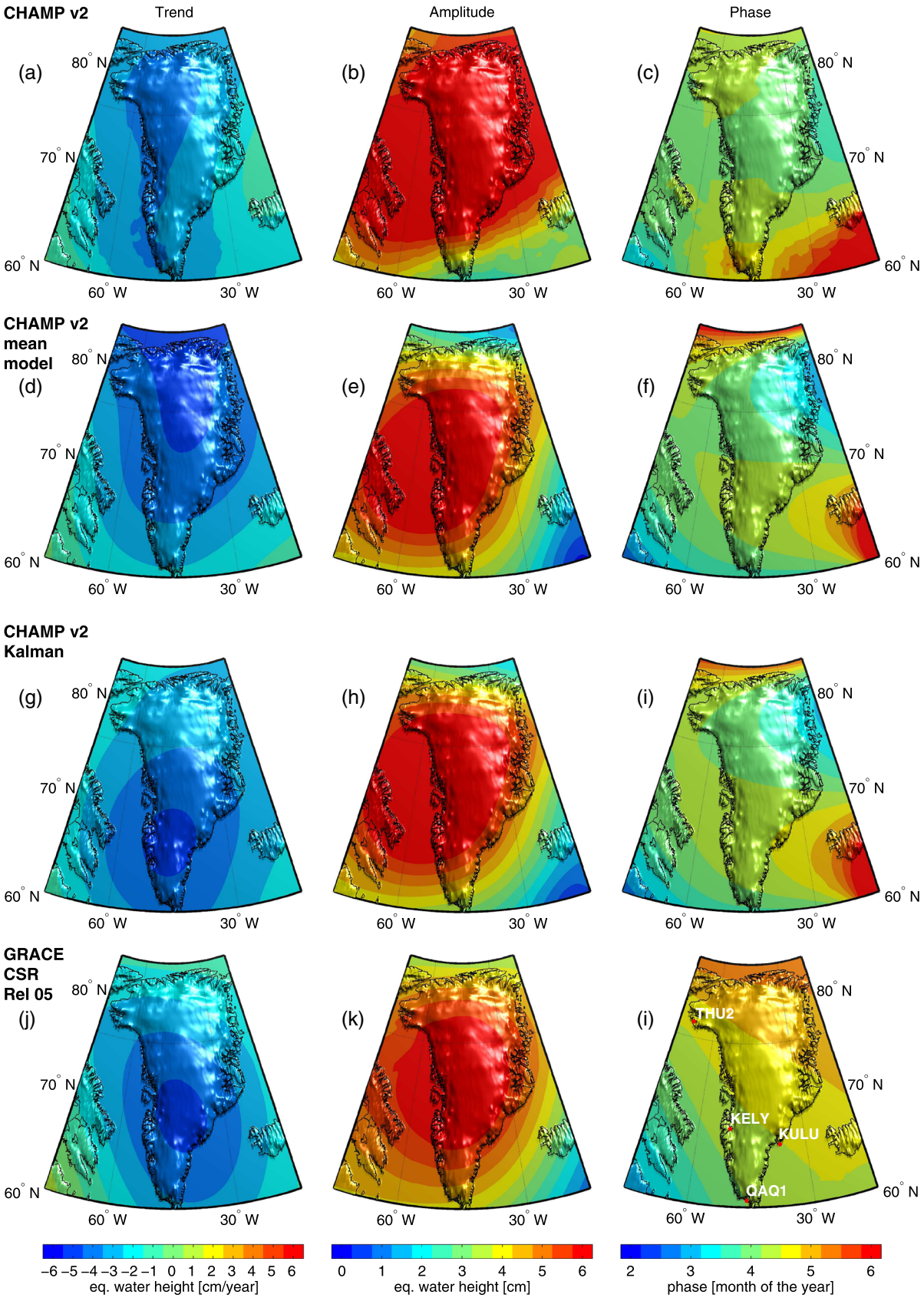

Figure 7. Trend, amplitude, and phase for (a–c) the CHAMP v2 solution, (d–f) the CHAMP v2 mean solution, (g–i) the CHAMP v2 Kalman solution, and (j–l) the GRACE (CSR and Rel05) in terms of equivalent water height; in Figure 7l, the locations of the four GPS stations used in section 3.3 are shown. The respective AOD1B-GAC products have been added.

Table 3. Signal RMS and Difference RMS With Respect to GRACE in Terms of Equivalent Water Height and Location of the Peak Value for the Solutions[a]

	RMS signal	RMS Δ_{GRACE}	Peak	Location	
Trend:	(cm/yr)	(cm/yr)	(cm/yr)	λ_P	ϕ_P
CHAMP v2	2.79	2.78	–3.60	50.4°W	66.0°N
CHAMP mean	3.70	1.54	–4.60	41.2°W	66.0°N
CHAMP Kalman	2.99	0.63	–4.36	46.1°W	66.0°N
GRACE	2.78	-	–4.39	42.1°W	69.2°N
Amplitude:	(cm)	(cm)	(cm)	λ_P	ϕ_P
CHAMP v2	6.53	1.75	8.87	44.6°W	71.2°N
CHAMP mean	4.84	0.66	6.75	56.2°W	69.7°N
CHAMP Kalman	4.97	0.54	6.81	56.1°W	70.1°N
GRACE	4.92	-	6.33	47.4°W	71.8°N
Phase:	(Month)	(Month)	-	-	-
CHAMP v2	4.27	0.71	-	-	-
CHAMP mean	4.16	0.76	-	-	-
CHAMP Kalman	4.24	0.72	-	-	-
GRACE	4.62	-	-	-	-

[a]In case of the trend, the peak is defined as the maximum negative value, whereas in case of the amplitude, it is the maximum positive value.

third and fourth rows for the readers convenience. There, the (visual) agreement between CHAMP and GRACE becomes much more evident and it demonstrates that CHAMP is able to see the strongest time-variable gravity field changes on land.

3.2. Greenland Time-Variable Gravity

[32] Observations of time-variable gravity field changes over land have benefited several research applications, e.g., hydrological or ice-mass change studies. In this section, we investigate the ability of hl-SST to provide useful ice-mass change data. One geographic region of particular interest for climate change studies is Greenland as the ice melting in that area may be an important indicator of the extent of global warming, cf. *Velicogna and Wahr* [2006]. For the subsequent analysis, the sum of the global atmospheric variability plus the oceanic pressure variability in terms of gravity (AOD1B-GAC product) [*Flechtner*, 2007] has been added back to the respective gravity field solutions in order to reduce differences arising from using different AOD products.

[33] First, the impact of the Kalman filter process is demonstrated for the Greenland area. Figure 7 shows four different solutions: Figures 7a–7c, the CHAMP v2; Figures 7d–7f, the CHAMP v2 mean model, which is also used for the prediction; Figures 7g–7i, the CHAMP v2 Kalman solution; and Figures 7j–7l, the GRACE solution. The corresponding statistics are shown in Table 3. Values are calculated as the area-weighted mean over the entire visible area.

[34] As expected and despite the Gaussian filtering of again 1000 km, the CHAMP v2 solution performs worst. The noise level does not allow us to observed realistic patterns. Only the phase is in good agreement with GRACE. The RMS of the phase shift is only 0.71 month equivalent to $\approx$ 20 days. In terms of the RMS, the phase of the other two CHAMP solutions do not produce better results but the visual pattern changes slightly.

[35] The most interesting aspect of the figure is certainly the comparison of the CHAMP v2 mean solution versus the CHAMP v2 Kalman solution. The pattern of the trend (Figures 7a, 7d, 7g, 7j) shows the strongest disagreement. The mean solution has a stronger trend in the northern part of Greenland. This is confirmed by the statistics in Table 3. The overall signal RMS is 2.99 cm/year for CHAMP and 2.78 cm/year for GRACE. The signal RMS is $\approx$ 23 % higher and also the difference RMS to GRACE is almost a factor 2.5 higher. The peak, i.e., maximum negative trend, is shifted further north. The comparison of the CHAMP solutions with the GRACE solutions shows that the Kalman solution produces the best agreement although the pattern is slightly rotated and shifted to the south-west. The magnitude of the peak is –4.36 cm/year in terms of equivalent water height, which is just $\approx$ 0.6% smaller than in case of GRACE.

[36] The amplitude pattern in Figures 7b, 7e, 7h, and 7k for the CHAMP v2 mean and the CHAMP v2 Kalman solution is almost identical. Only in the extreme north-eastern corner can we see a difference. In comparison to GRACE, the maxima are located further south-west and the maxima value is approximately $\approx$ 8 % higher. The location is nearly identical for both CHAMP solutions but shifted relative to GRACE by $\approx$ 9° to the west. The RMS difference is only slightly better for the CHAMP v2 Kalman solution, which is primarily due to an improved phase estimation in the north-east. There, a phase shift of up to 2 months occurs relative to GRACE, which can be reduced by the Kalman approach though it cannot be entirely removed.

[37] In conclusion, the Kalman approach reduces the noise considerably and it represents an important improvement for extracting a geophysically meaningful spatial pattern. The most benefit is achieved for the trend estimation. There is only a slight improvement in determining the annual amplitude. Better performance might be achievable in the future, but then the primary objective would be to improve the GPS positioning and the subsequent gravity field recovery. The Kalman filter is able to reduce the noise but depends on the signal to noise ratio in the time series of the spherical harmonic coefficients of the monthly solution. Improving the coefficients themselves will require improvements in the data processing at prior steps. Nevertheless, the agreement between the long-wavelength features of the trend and

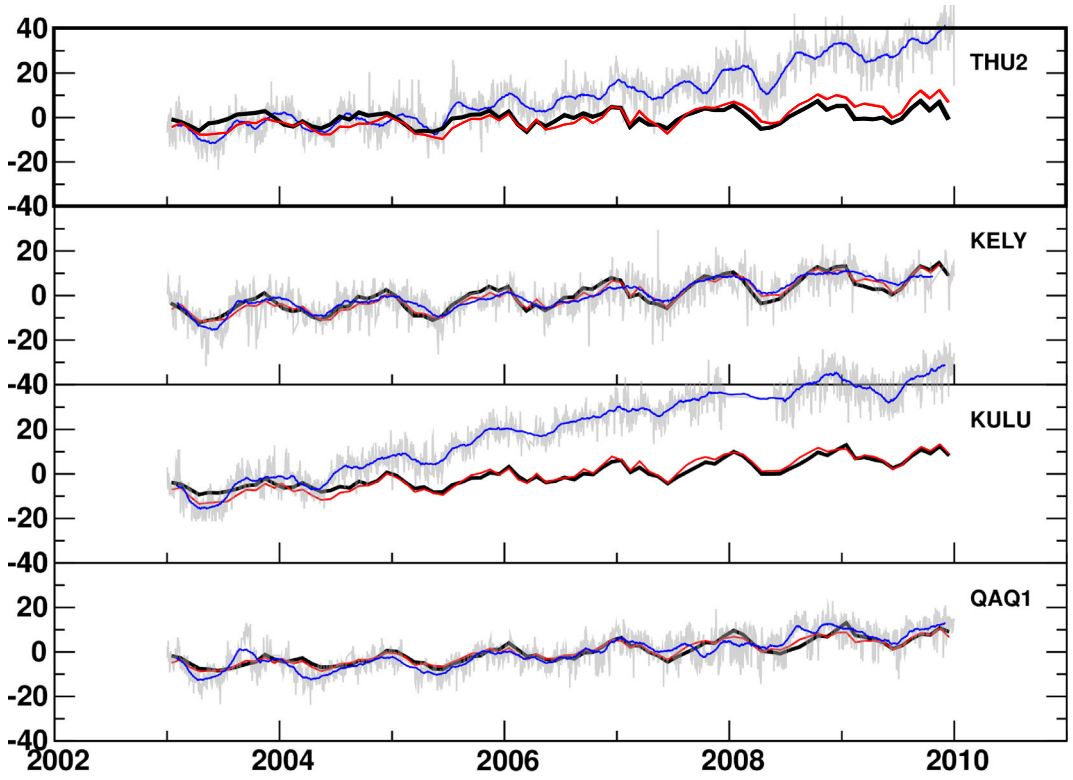

Figure 8. Estimates of surface displacements from gravity fields and observed GPS height coordinates at four locations in Greenland. Units are in millimeters. The thick black lines are the predicted up-coordinates estimated from the CHAMP data; the thin red lines are the GRACE data; the light-grey lines represent the daily GPS estimates; the thin blue lines represent 30 day averages of the daily GPS estimates.

the annual signal is exceptionally good between CHAMP and GRACE, especially when considering the reduced accuracy of the GPS observation (mm-level) with respect to the K-band observation (μm-level).

3.3. GPS Loading Analysis

[38] In this section, we convert the GRACE solutions and the CHAMP gravity fields to estimates of surface height changes. We only consider the CHAMP v2 Kalman solution that is referred to as the CHAMP solution for simplicity. Both the GRACE and CHAMP fields have had the atmospheric and ocean monthly dealiased fields added back in to make them consistent with the GPS data that contain the atmospheric and nontidal ocean loading signals. The degree-1 from *Swenson et al.* [2008] has also been added, and the coefficient $\bar{C}_{20}$ has been replaced by values derived from SLR [*Cheng and Tapley*, 2004]. To compute the vertical surface displacement dr due to the gravity field coefficients $\bar{C}_{lm}$ and $\bar{S}_{lm}$, we use equation (2) of *van Dam et al.* [2007]:

$$dr(\theta,\lambda) = R\sum_{l=1}^{\infty}\sum_{m=0}^{l}\frac{h_l}{1+k_l}W_l\bar{P}_{lm}\left[\bar{C}_{lm}\cos(m\lambda)+\bar{S}_{lm}\sin(m\lambda)\right] \quad (5)$$

where θ and λ are the spherical coordinates on the surface of the Earth, R the Earth radius, $\bar{P}_{lm}$ the associated Legendre functions of degree l and order m, with Love numbers h_l and k_l [*Han and Wahr*, 1995] in the Center of Figure reference frame [*Blewitt*, 2003], and Gaussian filter weighting coefficients W_l [*Wahr et al.*, 1998]. The radius of the filter has to be chosen differently than the way it was chosen in the previous section. The computation of surface displacements contains an additional aggregation step that can be thought of as a smoothing operator. Lower filter radii are possible and necessary since higher radii result in an over-smoothing and a loss of signal. Our tests showed that the best agreement with the GPS height coordinates are achieved for a smoothing radius of 500 km.

[39] Double-differenced ionosphere-free GPS data were processed using the GAMIT/GLOBK software version 10.4 [*Herring et al.*, 2010]. Observations below 15° were not included in order to minimize the effect of mismodeled low-elevation troposphere and antenna PCV (phase center variation) errors. Phase center offsets with azimuth-dependent and elevation-dependent absolute PCV corrections were applied. The antenna phase center model was applied using the igs08x model (IGSMAIL-6354,2011).

[40] The subsequent processing follows closely the procedure outlined in *Santamaría-Gómez et al.* [2012, section 3.1]. A priori zenith tropospheric delay values were applied using the Global Pressure and Temperature (GPT) model [*Boehm et al.*, 2007]. Residual zenith tropospheric delays were adjusted for every station assuming they were dominated by the unmodeled wet component. The estimated zenith wet delay was parameterized by a 2 h piecewise linear continuous model. The corresponding motions of the crust due to solid Earth and pole tides were corrected following

Table 4. Velocity Estimates From CHAMP, GRACE, and GPS for the Stations Thule (THU2), Kangerlussuaq (KELY), Kulusuk (KULU), and Qaqortoq (QAQ1)

	CHAMP (mm/yr)	GRACE (mm/yr)	GPS (mm/yr)
THU2	0.6 ± 0.2	2.0 ± 0.1	6.2 ± 0.0
KELY	2.4 ± 0.2	2.8 ± 0.1	2.7 ± 0.1
KULU	2.5 ± 0.2	3.1 ± 0.1	8.7 ± 0.0
QAQ1	2.1 ± 0.2	2.1 ± 0.1	2.9 ± 0.0

the International Earth Rotation and Reference Systems Service (IERS) Conventions [*McCarthy*, 2004]. Crustal motion due to the ocean tide loading was corrected by interpolating the tidal constituents for each station from the global grid of the FES2004 model [*Lyard et al.*, 2006]. Earth orientation parameters (pole position, rate, and UT1 rate) were estimated daily with a priori values from the IERS Bulletin A. Diurnal and semi-diurnal terms were added to the a priori UT1 and pole values. Orbital parameters were adjusted using 24 h arcs and taking the IGS reprocessed orbits as a priori values.

[41] The GLOBK software package was then used to generate daily station positions in ITRF08 [*Altamimi et al.*, 2011] of the 400+ sites used in this analysis. The height-coordinates for THU2 (Thule, Northwest Greenland), KELY (Kangerlussuaq, Western Greenland), KULU (Kulusuk, Southeast Greenland), and QAQ1 (Qaqortoq, Southern Greenland) are shown in Figure 8. The thick black lines are the predicted up-coordinates estimated from the CHAMP data; the thin red lines are the GRACE data; the light-grey lines represent the daily GPS estimates; and the thin blue lines represent 30 day averages of the daily GPS estimates.

[42] At the sites analyzed here, the CHAMP estimates are comparable in amplitude and trend with the GRACE estimates. The scatter of the differences are 5–7 mm. The best agreement is found for QAQ1 (5 mm RMS difference); the worst is KULU (7 mm RMS difference). The velocity estimates from CHAMP, GRACE, and GPS are shown in Table 4. The velocities from the three observations agree quite well at QAQ1 and KELY where the CHAMP heights match the GPS heights. At THU2 and KULU, the GPS data diverges from the satellite data, but also the CHAMP and GRACE estimated uplift velocities disagree the most. These accelerations in the GPS time series observed in the later years are broadly consistent with the space-time changes in ice mass presented in earlier studies using GRACE only [*Khan et al.*, 2007, 2010]. For THU2, the cause of the disagreement is still unclear. But the KULU GPS height-coordinate time series is known to be affected by the mass loss on the nearby Helheim Glacier [*Wahr et al.*, 2013; *Khan et al.*, 2007].

4. Conclusions

[43] We have shown that time-variable gravity field signals can be derived from hl-SST configurations alone. Two important data processing steps enabled the before never achieved recovery of trends for Greenland from CHAMP data without the need of combination with SLR observations and/or regularization. First, a thorough reprocessing of the GPS data provided a gain of 1 order of magnitude in sensitivity. The remaining noise is further reduced by applying a dedicated Kalman filtering. The time-variable pattern is restricted to the very long-wavelength features due to the reduced accuracy of the GPS observation with respect to the K-Band observation of GRACE. We used the refined data processing strategy to derive realistic trends and amplitudes for Greenland. The comparison to GPS ground stations shows very good agreement for the stations in Kangerlussuaq and Qaqortoq. In Thule and Kulusuk, the CHAMP solution agrees well with GRACE but GPS diverges which is likely caused by local phenomena invisible to the satellites. The research also shows that hl-SST cannot only serve as an alternative (at a lower spatial resolution) in case of the termination of GRACE but is also a viable source of information by itself. This is especially interesting in view of the upcoming three satellite Swarm constellation which promises a higher number of observations.

[44] **Acknowledgments.** We like to thank Drazen Švehla for providing the kinematic position data for the 2 years of CHAMP data used for the solution CHAMP v1. We also like to thank Franz Barthelmes and the staff at the ICGEM at the German Research Centre for Geosciences for hosting and providing public access to the data. Last but not least, we like to thank Tom Parsons, Frank Flechtner, and one anonymous reviewer for their helpful comments and suggestions.

References

Altamimi, Z., X. Collilieux, J. Legrand, B. Garayt, and C. Boucher (2007), ITRF2005: A new release of the International Terrestrial Reference Frame based on time series of station positions and Earth Orientation Parameters, *J. Geophys. Res.*, *112*, B09401, doi:10.1029/2007JB004949.

Altamimi, Z., X. Collilieux, and L. Métivier (2011), ITRF2008: An improved solution of the International Terrestrial Reference Frame, *J. Geod.*, *85*(8), 457–473, doi:10.1007/s00190-011-0444-4.

Beutler, G., A. Jäggi, L. Mervart, and U. Meyer (2010), The celestial mechanics approach: Theoretical foundations, *J. Geod.*, *84*(10), 605–624, doi:10.1007/s00190-010-0401-7.

Biancale, R., and A. Bode (2006), Mean annual and seasonal atmospheric tide models based on 3-hourly and 6-hourly ECMWF surface pressure data, *Tech. Rep. STR 06/01*.

Blewitt, G. (2003), Self-consistency in reference frames, geocenter definition, and surface loading of the solid Earth, *J. Geophys. Res.*, *108*(B2), 2103, doi:10.1029/2002JB002082.

Bock, H., R. Dach, A. Jäggi, and G. Beutler (2009), High-rate GPS clock corrections from CODE: Support of 1 Hz applications, *J. Geod.*, *83*(11), 1083–1094, doi:10.1007/s00190-009-0326-1.

Bock, H., A. Jäggi, U. Meyer, P. Visser, J. Ijssel, T. Helleputte, M. Heinze, and U. Hugentobler (2011), GPS-derived orbits for the GOCE satellite, *J. Geod.*, *85*(11), 807–818, doi:10.1007/s00190-011-0484-9.

Boehm, J., R. Heinkelmann, and H. Schuh (2007), Short Note: A global model of pressure and temperature for geodetic applications, *J. Geod.*, *81*(10), 679–683, doi:10.1007/s00190-007-0135-3.

Cheng, M. K., B. Gunter, J. C. Ries, D. P. Chambers, and B. D. Tapley (2002), Temporal variations in the Earth's gravity field from SLR and CHAMP GPS data, in *Gravity and Geoid: Proceedings of 3rd Meeting of the International Gravity and Geoid Commission*, edited by I. N. Tziavos, pp. 237–242, Ziti, Thessaloniki, Greece.

Cheng, M. K., and B. D. Tapley (2004), Variations in the Earth's oblateness during the past 28 years, *J. Geophys. Res.*, *109*, B09402, doi:10.1029/2004JB003028.

Dach, R., E. Brockmann, S. Schaer, G. Beutler, M. Meindl, L. Prange, H. Bock, A. Jäggi, and L. Ostini (2009), GNSS processing at CODE: Status report, *J. Geod.*, *83*(3-4), 353–365, doi:10.1007/s00190-008-0281-2.

Davis, J. L., B. P. Wernicke, and M. E. Tamisiea (2012), On seasonal signals in geodetic time series, *J. Geophys. Res.*, *117*, 1–10, doi:10.1029/2011JB008690.

Dow, J., R. Neilan, and G. Gendt (2005), The International GPS Service: Celebrating the 10th anniversary and looking to the next decade, *Adv. Space Res.*, *36*(3), 320–326, doi:10.1016/j.asr.2005.05.125.

European Space Agency (1999), Gravity field and steady-state ocean circulation mission, Eur. Space Agency Rep. ESA SP-1233(1), edited by B. Battrick, 217 pp.

European Space Agency (2004), The Earth's magnetic field and environment explorers, Eur. Space Agency Rep. ESA SP-1279(6), edited by B. Battrick, 70 pp.

Flechtner, F. (2007), AOD1B Product Description Document for Product Releases 01 to 04, Rev. 3.1, April 13, 2007, GRACE project document, 327–750.

Flechtner, F., P. Morton, M. Watkins, and F. Webb (2013), Status of the GRACE follow-on mission, *Proceedings of the International Association of Geodesy Symposia Gravity, Geoid and Height System (GGHS2012), 9.-11.10.2012*, Venice, Italy, IAGS-D-12-00141, (accepted).

Gelb, A. (1974), *Applied Optimal Estimation*, 374 pp., MIT Press, Cambridge, Mass.

Han, D., and J. Wahr (1995), The viscoelastic relaxation of a realistically stratified Earth, and a further analysis of postglacial rebound, *Geophys. J. Int.*, *120*(2), 287–311, doi:10.1111/j.1365-246X.1995.tb01819.x.

Heiskanen, W., and H. Moritz (1967), *Physical Geodesy*, 364 pp., W. H. Freeman, San Francisco, Calif.

Herring, T. A., R. W. King, and S. C. McClusky (2010), GAMIT: Reference Manual Version 10.34, *Tech. Rep.*, Mass. Inst. of Technol., Cambridge.

Hugentobler, U. (2004), CODE high rate clocks, *IGS Mail No. 4913*, IGS Central Bureau Information System.

Jäggi, A., R. Dach, O. Montenbruck, U. Hugentobler, H. Bock, and G. Beutler (2009), Phase center modeling for LEO GPS receiver antennas and its impact on precise orbit determination, *J. Geod.*, *83*(12), 1145–1162, doi:10.1007/s00190-009-0333-2.

Khan, S. A., J. Wahr, L. A. Stearns, G. S. Hamilton, T. van Dam, K. M. Larson, and O. Francis (2007), Elastic uplift in southeast Greenland due to rapid ice mass loss, *Geophys. Res. Lett.*, *34*, L21701, doi:10.1029/2007GL031468.

Khan, S. A., J. Wahr, M. Bevis, I. Velicogna, and E. Kendrick (2010), Spread of ice mass loss into northwest Greenland observed by GRACE and GPS, *Geophys. Res. Lett.*, *37*, L06501, doi:10.1029/2010GL042460.

Lin, T., C. Hwang, T.-P. Tseng, and B. Chao (2012), Low-degree gravity change from GPS data of COSMIC and GRACE satellite missions, *J. Geodyn.*, *53*, 34–42, doi:10.1016/j.jog.2011.08.004.

Lyard, F., F. Lefevre, T. Letellier, and O. Francis (2006), Modelling the global ocean tides: Modern insights from FES2004, *Ocean Dyn.*, *56*(5-6), 394–415, doi:10.1007/s10236-006-0086-x.

Mayer-Gürr, T., K. Ilk, A. Eicker, and M. Feuchtinger (2005), ITG-CHAMP01: A CHAMP gravity field model from short kinematic arcs over a one-year observation period, *J. Geod.*, *78*(7-8), 462–480, doi:10.1007/s00190-004-0413-2.

McCarthy, D. D. (2004), IERS Conventions (2003), *Tech. Rep. No. 32*, Verlag des Bundesamts für Kartographie und Geodäsie.

Pavlis, N. K., S. A. Holmes, S. C. Kenyon, and J. K. Factor (2012), The development and evaluation of the Earth Gravitational Model 2008 (EGM2008), *J. Geophys. Res.*, *117*, B04406, doi:10.1029/2011JB008916.

Petit, G., and B. Luzum (2010), IERS conventions (2010), *Tech. Rep. 36*, Verlag des Bundesamts für Kartographie und Geodäsie.

Prange, L. (2010), Global gravity field determination using the GPS measurements made onboard the low Earth orbiting satellite CHAMP, PhD thesis, Geodätisch-geophysikalische Arbeiten in der Schweiz, vol. 81, http://www.sgc.ethz.ch/sgc-volumes/sgk-81.pdf.

Qiang, Z., and P. Moore (2005), On the contribution of CHAMP to temporal gravity field variation studies, in *Earth Observation With CHAMP, Results From Three Years in Orbit*, edited by C. Reigber et al., pp. 19–24, Springer, Berlin.

Reigber, C., H. Lühr, and P. Schwintzer (2001), Announcement of opportunity for CHAMP, *Tech. Rep. CH-GFZ-AO-001*.

Reubelt, T. (2008), Harmonische Gravitationsfeldanalyse aus GPS- vermessenen kinematischen Bahnen niedrig fliegender Satelliten vom Typ CHAMP, GRACE und GOCE mit einem hoch auflösenden Beschleunigungsansatz, PhD thesis, Universität Stuttgart.

Santamaría-Gómez, A., M. Gravelle, X. Collilieux, M. Guichard, B. M. Míguez, P. Tiphaneau, and G. Wöppelmann (2012), Mitigating the effects of vertical land motion in tide gauge records using a state-of-the-art GPS velocity field, *Global Planet. Change*, *98-99*, 6–17, doi:10.1016/j.gloplacha.2012.07.007.

Schaer, S., and R. Dach (2008), Model changes made at CODE, *IGS Mail No. 5771*, IGS Central Bureau Information System.

Schmid, R., P. Steigenberger, G. Gendt, M. Ge, and M. Rothacher (2007), Generation of a consistent absolute phase-center correction model for GPS receiver and satellite antennas, *J. Geod.*, *81*(12), 781–798, doi:10.1007/s00190-007-0148-y.

Sneeuw, N., C. Gerlach, D. Svehla, and C. Gruber (2002), A first attempt at time-variable gravity recovery from CHAMP using the energy balance approach, in *Gravity and Geoid: Proceedings of 3rd Meeting of the International Gravity and Geoid Commission*, edited by I. N. Tziavos, pp. 237–242, Ziti, Thessaloniki, Greece.

Steigenberger, P., M. Rothacher, R. Dietrich, M. Fritsche, A. Rülke, and S. Vey (2006), Reprocessing of a global GPS network, *J. Geophys. Res.*, *111*, B05402, doi:10.1029/2005JB003747.

Švehla, D., and M. Rothacher (2005), Kinematic precise orbit determination for gravity field determination, in *A Window on the Future of Geodesy, Int. Assoc. of Geod. Symp.,* vol. 128, pp. 181–188, Springer, Berlin, doi:10.1007/3-540-27432-4_32.

Swenson, S., D. Chambers, and J. Wahr (2008), Estimating geocenter variations from a combination of GRACE and ocean model output, *J. Geophys. Res.*, *113*, B08410, doi:10.1029/2007JB005338.

Tapley, B. D., et al. (1996), The Joint Gravity Model 3, *J. Geophys. Res.*, *101*(B12), 28,029–28,049, doi:10.1029/96JB01645.

Tapley, B. D., S. Bettadpur, J. C. Ries, P. F. Thompson, and M. M. Watkins (2004), GRACE measurements of mass variability in the Earth system, *Science*, *305*(5683), 503–5, doi:10.1126/science.1099192.

van Dam, T., J. Wahr, and D. Lavallée (2007), A comparison of annual vertical crustal displacements from GPS and Gravity Recovery and Climate Experiment (GRACE) over Europe, *J. Geophys. Res.*, *112*, B03404, doi:10.1029/2006JB004335.

Velicogna, I., and J. Wahr (2006), Acceleration of Greenland ice mass loss in spring 2004, *Nature*, *443*(7109), 329–31, doi:10.1038/nature05168.

Wahr, J., M. Molenaar, and F. Bryan (1998), Time variability of the Earth's gravity field: Hydrological and oceanic effects and their possible detection using GRACE, *J. Geophys. Res.*, *103*(B12), 30,205–30,229, doi:10.1029/98JB02844.

Wahr, J., T. Kahn, T. van Dam, L. Liu, J. H. van Angelen, M. R. van den Broeke, and C. M. Meertens (2013), The use of GPS horizontals for loading studies, with applications to northern California and southeast Greenland, *J. Geophys. Res. Solid Earth*, *118*, 1795–1806, doi:10.1002/jgrb.50104.

Weigelt, M. L. (2007), Global and local gravity field recovery from satellite-to-satellite tracking, PhD thesis, Univ. of Calgary.

Weigelt, M., N. Sneeuw, E. J. O. Schrama, and P. N. A. M. Visser (2013), An improved sampling rule for mapping geopotential functions of a planet from a near polar orbit, *J. Geod.*, *87*(2), 127–142, doi:10.1007/s00190-012-0585-0.

Zumberge, J. F., M. B. Heflin, D. C. Jefferson, M. M. Watkins, and F. H. Webb (1997), Precise point positioning for the efficient and robust analysis of GPS data from large networks, *J. Geophys. Res.*, *102*(B3), 5005–5017, doi:10.1029/96JB03860.